

1 **First ‘in situ’ determination of gas transport coefficients (D_{O_2} , D_{Ar} and D_{N_2}) from bulk gas**
2 **concentration measurements (O_2 , N_2 , Ar) in natural sea ice .**

3 Odile Crabeck^{1*}, Delille.B², Rysgaard.S^{1,3,4}, Thomas.D.N^{6,7}, Geilfus.N-X^{1,3}, Else.B¹, Tison J-L⁵.

4 ^{1.} Department of Geological science, CEOS, University of Manitoba, Canada

5 ^{2.} Unité d’océanographie chimique, MARE, Université de Liège, Belgium

6 ^{3.} Arctic Research Centre, Aarhus University, C.F. Denmark

7 ^{4.} Greenland Climate Research Centre, Greenland Institute of Natural Resources, Kivioq 2., 3900 Nuuk,
8 Greenland

9 ^{5.} Laboratoire de glaciologie, DSTE, Université Libre de Bruxelles, Belgium

10 ^{6.} School of Ocean Sciences, Bangor University, Menai Bridge, Anglesey. U.K.

11 ^{7.} Marine Research Centre, Finnish Environment Institute, Helsinki, Finland.

12 * Corresponding author: Odile Crabeck, Department of Geological science, CEOS, University of Manitoba,
13 Canada, crabecko@myumanitoba.ca

14 **Abstract**

15 We report bulk gas concentrations of O_2 , N_2 and Ar , as well as their transport coefficients, in
16 natural landfast subarctic sea ice in southwest Greenland. The observed bulk ice gas composition
17 was 27.5% O_2 , 71.4% N_2 and 1.09% Ar . Most previous studies suggest that convective transport
18 is the main driver of gas displacement in sea ice and have neglected diffusion processes.
19 According to our data, brines were stratified within the ice, so that no convective transport could
20 occur within the brine system. Therefore, diffusive transport was the main driver of gas
21 migration. By analysing the temporal evolution of an internal gas peak within the ice, we deduced
22 the bulk gas transport coefficients for oxygen (D_{O_2}), argon (D_{Ar}) and nitrogen (D_{N_2}). The values
23 fit to the few existing estimates from experimental work, and are close to the diffusivity values in
24 water ($10^{-5} \text{ cm}^2 \text{ s}^{-1}$). We suggest that gas bubbles escaping from the brine to the atmosphere - as

25 the ice gets more permeable during melt - could be responsible for the previously reported high
26 transport coefficients. These results underline that when there is no convective transport within
27 the sea ice, the transport of gas by diffusion through the brines, either in the liquid or gaseous
28 phases, is a major factor in controlling the ocean–atmosphere exchange.

29

30 **Keywords:** Sea ice, gas, diffusion, transport, Greenland.

31 **1. Introduction**

32 To date, only a limited number of studies describing the natural gas composition of sea ice are
33 available [e.g. *Matsuo and Miyake*, 1966; *Rysgaard and Glud*, 2004; *Tison et al.*, 2002; *Zhou et*
34 *al.*, 2013]. These studies typically found a total gas content lower than 23.75 ml STP kg⁻¹ ice – a
35 value expected if seawater is instantly frozen – and reported bulk ice gas compositions on the
36 order of $\approx\frac{1}{3}$ O₂ and $\approx\frac{2}{3}$ N₂, similar to atmospheric and seawater compositions. The formation of
37 these gas inclusions has been described in detail by *Tsurikov*, [1979] who identified nine key
38 processes that trap gases in sea ice. Most importantly, during the freezing process the expelled
39 dissolved gases are trapped in the brines, or in bubbles that are released at the ice-water interface
40 (Figure 1: initial gas entrapment). Increased concentrations of solutes in brines by freezing results
41 in further formation of gas bubbles by nucleation processes (Figure 1: post genetic process).
42 More gas inclusions can be created during sea ice melt, as water vapour forms inside the brine
43 pockets above the freeboard line. Finally, drained brine pockets and channels may be replaced by
44 atmospheric gases.

45

46 The presence of a gas phase in sea ice creates the potential for gas exchange with the atmosphere,
47 although unfortunately gas transfer at the sea ice-atmosphere interface is not well constrained

48 [Else *et al.*, 2011; Heinesch *et al.*, 2010; Loose *et al.*, 2011; Miller *et al.*, 2011; Papakyriakou and
49 Miller, 2011; Sørensen *et al.*, 2013; Zemmeling *et al.*, 2006]. For example, studies have shown
50 that sea ice can act as a source [e.g. Geilfus *et al.*, 2012, 2013; Miller *et al.*, 2011; Nomura *et al.*,
51 2006] or a sink for atmospheric CO₂ [e.g. Nomura *et al.*, 2010; Papadimitriou *et al.*, 2012;
52 Rysgaard *et al.*, 2007; Zemmeling *et al.*, 2006], with the reported fluxes spanning several orders
53 of magnitude.

54
55 Three main processes should be considered for gas transport within sea ice (Figure 1: transport):
56 a) convection with the brine medium, b) diffusion along the concentration gradient (in the
57 dissolved state within the brine medium) and c) upward gas movement under buoyancy (in the
58 gaseous state within the brine medium). All three require that there is a certain level of
59 permeability in the sea ice, which may differ depending on the process considered. According to
60 Golden *et al.* [1998, 2007], the permeability of sea ice rapidly increases when the brine volume
61 fraction exceeds 5%. At brine volume fractions below 5% no brine convection is expected to
62 occur, and the ice cover is often considered impermeable to gas exchange. A recent study by
63 Zhou *et al.* [2013] suggests that a brine volume of ca. 7% is required for upward bubble
64 migration (through bubble buoyancy). These observations are consistent with Loose *et al.* [2011]
65 who suggest that the permeability threshold for gas transport could be different from the
66 permeability threshold for brine convection (i.e. gravity drainage) or bubble migration. Past
67 studies [Gosink *et al.*, 1976; Loose *et al.*, 2009, 2011; Shaw *et al.*, 2011] have actually suggested
68 that diffusion is the major control on gas fluxes across sea ice, and it appears to be active even at
69 low brine volumes. Diffusive transport through the porous structure of sea ice is therefore an
70 alternative pathway for ocean–atmosphere exchange of gases in the absence of convection
71 processes (i.e. brine drainage under brine density instability).

72

73 The aim of the present study was to examine the physical processes that affect mass transport of
74 biogenic gases across and within sea ice. Unlike previous studies, which have used artificial gas
75 tracers [e.g. *Gosink et al.*, 1976], or artificial sea ice [e.g. *Loose et al.*, 2011], we used
76 measurements of natural gas concentrations in natural sea ice samples. By studying the temporal
77 evolution of the vertical profile of O₂, N₂, and Ar, we were able to compute diffusivities of these
78 gases in a natural environment. Since only one study [*Gosink et al.*, 1976] reports such
79 measurements in natural environment, our findings significantly enhance scientific understanding
80 of gas transport in sea ice. Furthermore, our observations can be used to validate previous studies
81 made in the laboratory and other experimental settings.

82 **2. Study site**

83 The sampling was conducted from 10 to 16 March 2010 on first-year land-fast sea ice in Kapisillit
84 in the vicinity of Nuuk, SW Greenland (64°26'N 50°13'W, Figure 2). To follow the temporal
85 evolution of the sea ice, we sampled sea ice and the underlying water column four times at the
86 same site on three occasions: 11 March, 13 March and 15 March. Sampling was performed
87 within an area of about 25 m² in order to minimize bias from spatial heterogeneity. The water
88 depth at the location ranged from 40 to 45 m, and the mean salinity of seawater in the Kapisillit
89 fjord was 32. The air temperatures during the study period ranged from -8.8 °C to +2.9 °C
90 (average -3.2 °C). The survey took place before the onset of the spring algal bloom:
91 Concentrations of chlorophyll-a were $2.8 \pm 0.4 \mu\text{g L}^{-1}$ (SE, n = 3) in the bottom 12 cm of ice,
92 while the average concentration across the entire ice thickness was $1.0 \pm 1.2 \mu\text{g L}^{-1}$ (SE, n=3)
93 [*Long et al.*, 2012; *Søgaard et al.*, 2013].

94 **3. Methods**

95 **3.1 *Sea ice temperature, salinity and texture:***

96 Ice cores were extracted using a stainless-steel corer with an internal diameter of 9 cm (Kovacs
97 Ent., Lebanon, USA). Cores were immediately wrapped in polyethylene bags and stored at the
98 sampling site in an insulated box filled with individual cooling bags pre-cooled at -20°C. In the
99 laboratory, ice cores were kept at -20°C in the dark to ensure brine/gas immobilization and to
100 inhibit biological processes [Eicken, 1991]. On a replicate core extracted from the same location,
101 *in situ* ice temperature was measured with a depth resolution of 5 cm, using a calibrated probe
102 (Testo 720) inserted into pre-drilled holes (with the same diameter as the probe), perpendicular to
103 the ice core axis. The precision of the probe was ± 0.1 °C. This ‘temperature’ ice core was
104 immediately cut into 5 cm slices, stored in polyethylene buckets, and left to melt. Back in the
105 laboratory, bulk ice salinity was measured with a portable conductivity meter (Orion Star Series
106 Meter WP-84TP) with a precision of ± 0.1 . To describe the texture of the ice, horizontal thin
107 sections were produced in 10 cm sections from a third ice core, using the standard microtone
108 (Leica SM2400) following the procedure described by Langway [1958] and Tison *et al.* [2008].
109 The images from horizontal thin sections were collected with a digital camera (Nikon Coolpix
110 S200, 7.1 megapixels) between crossed polarisers.

111

112 **3.2 *Total gas content***

113 The total volume of gas within sea ice (content in mL STP of gas per kg of ice) was measured
114 with a resolution of 5 cm using the wet extraction method [Raynaud *et al.*, 1982]. In short, ice
115 samples from the retained core were placed in an evacuated glass container. The ice was then
116 melted and refrozen from the bottom using a -70°C cold ethanol bath. This technique of melting-

117 refreezing releases both the dissolved gas in the brine and the gas content from the bubbles [*Tison*
118 *et al.*, 2002]. After the refreezing, the container was connected to a Toepler pump extraction
119 system, and the entire gas volume was directed through a pre-vacuumed line to a mercury-
120 graduated burette. Knowing the exact weight of the sample analyzed, the ice temperature, and
121 atmospheric pressure, we calculated the STP gas content of the sample with a precision of $\pm 5\%$.

122 **3.3 Gas composition**

123 Argon (Ar), oxygen (O₂) and nitrogen (N₂) were analyzed by gas chromatography. Extraction of
124 the gas phase from the ice used the dry-crushing technique as developed for gas measurements in
125 continental ice [*Raynaud et al.*, 1982]. Each ice core was cut in successive 5 cm sections, and 60
126 g of each section was put into a vessel together with stainless steel beads. The vessel was
127 evacuated to 10^{-3} torr, and then fixed to an ice crusher as described in *Raynaud et al.* [1982] and
128 *Stefels et al.* [2012]. The stainless steel beads impact the ice block during the shaking process, so
129 that the ice is crushed into a fine powder. The cutting and shaking processing took place in a cold
130 room at - 25 °C. After crushing, the vessel was kept at - 50°C in a cold ethanol bath, and
131 connected to a gas chromatograph equipped with a thermal conductivity detector for
132 concentration analyses [*Skoog et al.*, 1997]. We used AlphagazTM2 He (Air Liquid –P0252) as
133 the carrier gas, and a 22 ml packed column (Mole Sieve 5A 80/100; 5m x 1/8”). The gas
134 collected included both the gas bubbles in the ice, and the dissolved phase within liquid brines.

135
136 We compared the evolution of Ar, O₂, and N₂ concentration in bulk ice to the inventory
137 constrained by the solubility in brine at atmospheric saturation. The latter represents the
138 maximum concentration of Ar, O₂ and N₂ in the dissolved phase, if no super-saturation existed in
139 the brine [*Carte*, 1961; *Lubtkin*, 2003, *Zou et al.*, 2013]. It is obtained by calculating the

140 temperature and salinity dependent solubility of Ar, O₂ and N₂ in the brines [*Garcia and Gordon,*
141 1992; *Hamme and Emerson, 2004*] and dividing it by the relative brine volume (brine volume
142 fraction b/V , see below) to express it as micromoles per litre of bulk ice. *Zhou et al.* [2013]
143 showed that these relationships remain valid for the range of temperature and salinity found in
144 sea ice. The difference between observed concentration in bulk ice ($C_{bulk\ ice}$) and the theoretical
145 saturation concentration in brine ($C_{saturation}$) provides a maximum estimate of the gas
146 concentration in the ice that resides in the gas phase, C_B (i.e. the gas content of bubbles, assuming
147 no super saturation in the brines):

$$148 \quad C_B = C_{bulk\ ice} - C_{saturation} \quad (1)$$

149 We also calculated the supersaturation factor, (Sat_f):

$$150 \quad Sat_f = C_{bulk\ ice} / C_{saturation} \quad (2)$$

151 and the percent gas content in the bubbles, (f_B):

$$152 \quad f_B = \left(C_B / C_{bulk\ ice} \right) \times 100 \quad (3)$$

153

154 **3.4 Liquid/gas filled porosity and Rayleigh number**

155 The brine volume, (b), was calculated according to *Cox and Weeks* [1983] for ice temperature < -
156 2 °C and according to *Leppäranta and Manninen* [1988] for ice temperature \geq -2 °C, neglecting
157 the gas filled porosity. Brine salinity, (S_b), was calculated from the measured sea ice temperatures
158 and freezing point of seawater [*UNESCO, 1978*]. The brine volume fraction or gas filled porosity,
159 (V_b), was calculated as brine volume/bulk sea ice volume (b/V , expressed in %).

160 The bubble volume (L gas phase per L of ice), (B), was determined by multiplying C_B by the gas
161 molar volume using gas law normalised at the average ice temperature (-3.2 °C) ($V_m = 22.14 \times$
162 10^{-6} L mol⁻¹), and summing the contribution of all gas species:

163
$$B = C_B \times Vm \quad (4)$$

164 The gas filled porosity or bubble volume fraction was calculated as a percentage of the volume
165 total of ice, V_B :

166
$$V_B = \left(\frac{B}{\text{Bulk ice volume}} \right) \times 100 \quad (5)$$

167 This calculated value is a maximum percentage, supposing that no supersaturation existed in the
168 brines, and only considering O_2 , N_2 and Ar concentrations in the ice. Note also that this value is
169 slightly underestimated since C_B is calculated from $C_{saturation}$ (equation (1)), itself
170 overestimated since we neglected the gas filled porosity in the use of *Cox and Weeks* [1983]
171 formulation to estimate the brine volume fraction. *Cox and Weeks* [1983] estimated the gas filled
172 porosity to be between 1% to 5%.

173
174 The Rayleigh number is a parameter that primarily determines the onset of convection (e.g.
175 gravity drainage) and provides information about the vertical stability in the brine system. The
176 Rayleigh number (Ra) was estimated using the definition of *Notz and Worster* [2008].

177 **4 Results**

178 **4.1 Physical ice properties**

179 Detailed physical properties of the sea ice cores are presented elsewhere [*Crabeck et al., 2014*;
180 *Kaartokallio et al., 2013*; *Søgaard et al., 2013*]. In short, the ice consisted of columnar crystals,
181 and was relatively warm throughout, with a slight temperature gradient (Figure 3a) from top (-2.8
182 to -3.8 °C) to bottom (-0.8 to -1.2°C). The ice was covered by a thin layer of frozen snow, less
183 than 3 cm thick during all the sampling period. The average bulk ice salinity was 3.2, and the ice
184 salinity profiles deviated from the classical C-shape due to a variable localised riverine input

185 (Figure 3b). During the survey, the brine volume fraction fell below the permeability
186 threshold of 5% at various depths (Figure 3c), indicating that the atmosphere was not effectively
187 connected to the seawater through the ice. Furthermore, the Rayleigh number ranged from 0 to
188 0.3 (Figure 3d), and remained well below the theoretical convection threshold of 5
189 [Vancoppenolle *et al.*, 2010] or 10 [Notz and Worster, 2008] throughout the ice. Thus, we do
190 not expect that convective transport of brine occurred at anytime, or at any level of the sea
191 ice. However, the V_b exceeds 30% in the bottom of the ice (Figure 3c), and there was no
192 brine convection because the driving buoyancy given by the brine density gradient was not
193 large enough to overcome dissipation.

194 **4.2 Gas composition**

195 At all dates, the total gas content in sea ice ranged from 4 to 23.2 ml STP kg^{-1} ice, consistently
196 lower than the 23.75 ml STP kg^{-1} ice expected for instantly frozen seawater [Cox and Weeks,
197 1983]. This is consistent with past findings [e.g. Tison *et al.*, 2002], and is a result of the rejection
198 of gases during ice formation. Furthermore, a peak in gas content in the ice was observed
199 between 25 cm and 35 cm below the surface at all sampling dates (Figure 4a).

200
201 Mixing ratios in sea ice ranged from 0.94% to 1.29% for Ar, 22.4% to 32.9% for O_2 , and 68.9 to
202 76.6% for N_2 (Table 1). These correspond to a bulk ice Ar concentration of 1.3 - 11.7 $\mu\text{mol L}^{-1}$
203 ice (average 5.4 $\mu\text{mol L}^{-1}$ ice), a bulk ice O_2 concentration of 40 - 275 $\mu\text{mol L}^{-1}$ ice (average 132
204 $\mu\text{mol L}^{-1}$ ice) and a bulk ice N_2 concentration of 57 - 830 $\mu\text{mol L}^{-1}$ ice (average 354 $\mu\text{mol L}^{-1}$ ice).
205 Each gas profile (for each sampling date) had minimum concentrations in the bottom of the sea
206 ice and a peak around 27 cm below the ice surface (Figure 5). Over time the O_2 , N_2 and Ar gas

207 peaks decreased. Between 11 and 13 March, O₂ and Ar concentrations decreased by 13.9 and
208 13.6%, respectively, while N₂ concentrations decreased 3 times faster (32.1%).

209
210 Each gas species exceeded the concentrations calculated at atmospheric saturation (Table 2). The
211 saturation factor (Sat_f) (equation 2) varied from 0.82 to 39 for N₂, from 0.64 to 20.2 for O₂ and
212 from 0.52 to 18.5 for Ar. Maximum supersaturation factors were systematically observed in the
213 middle of the ice, 27.5 cm below the ice surface, while the minimum was observed in the
214 permeable bottom 5 cm of the ice (Table A1). N₂ was the most supersaturated gas species, with
215 an average saturation factor of 9.16, compared to 6.88 for O₂ and 5.05 for Ar. According to
216 equation (3), more than 70% of the gas species were in the gas phase while less than 30% was
217 dissolved in the brine (Table A1).

218
219 Overall, the liquid filled porosity represented 3 to 8% of the ice volume (Table A1), except in the
220 bottom 5 cm where V_b exceeded 30%. The calculated gas filled porosity was at most 2.2% of the
221 ice volume, and it was equal, or close to, 0 in the bottom 5 cm. This means that all gas species
222 were dissolved in the brine in the bottom horizons of the sea ice. The total porosity varied from 4
223 to 12%, except in the bottom 5 cm where it exceeded 30%.

224 **5 Discussion**

225 **5.1 Gas profiles**

226 All sampling dates showed a peak of gas content between 25 and 35 cm depth, which decreased
227 over time. As the fjord is periodically influenced by riverine input [*Mortensen et al.*, 2011] this
228 layer could be formed during periods with freshwater flowing under the growing ice. This

229 would create fresher less permeable ice layers and at the same time increase the total gas
230 content due to the higher gas content in freshwater relative to seawater (Figure 3a. and
231 Figure 5).

232
233 Gas profiles in sea ice result from both physical and/or biological processes. Ar is an inert gas
234 and therefore is not involved in biogeochemical processes, and so it can be used as a tracer of
235 physical processes involved in gas concentration and transport within sea ice [Zhou *et al.*, 2013].
236 In contrast, O₂ and N₂ are biogenic gases and their dynamics involve both physical and
237 biogeochemical processes. In seawater, the Ar:O₂ ratio is commonly used to remove the physical
238 contribution to oxygen supersaturation, and to determine the biological oxygen production [e.g;
239 Cassar *et al.*, 2009; Castro-Morales *et al.*, 2013]. However, the strong correlation ($r^2 > 0.89$,
240 $P \leq 0.01$) between Ar and both O₂ and N₂ in this study (Figure 6), suggests that physical transport
241 processes mainly controlled the gas compositions within the sea ice, biological processes only
242 having a minor effect. These observations are in agreement with the abiotic laboratory sea ice
243 experiment described by Tison *et al.* [2002]. In addition, Sørensen *et al.* [2013] have shown that
244 the total dissolved inorganic carbon within the ice cover in the same area was mainly controlled
245 by physical export via brine drainage and the precipitation/dissolution of calcium carbonate
246 rather than biological processes.

247
248 The relative proportion of O₂, Ar and N₂ in bulk sea ice in this study are intermediate between the
249 relative gas composition in dissolved seawater and the atmospheric gas composition (Table 1 and
250 Figure 6). These results are in agreement with the past studies of Matsuo and Miyake [1966] and
251 Tison *et al.* [2002] and reflect the mixed contribution of the dissolved and gaseous fractions of
252 each gas, with the dominance of the gaseous (bubble) fraction (as also shown by the regression

253 line in Figure 6 being closer to the atmospheric ratio and the f_B values in Table A1). Each gas
254 species in the bottom ice layers was close to, or below, atmospheric saturation (Figure 5),
255 confirming the results of *Zhou et al.* [2013] that the gas incorporation at the ice water interface
256 occurs close to the atmospheric solubility value.

257
258 The ice was enriched in N_2 (i.e. highest saturation factor) compared to O_2 and Ar (Table 2). The
259 gas composition is a function of a chemical separation of gases diffusing across the boundary
260 layer at the ice-water interface during the ice growth [*Carte*, 1961; *Killawee et al.*, 1998; *Loose et*
261 *al.*, 2009, 2011; *Tison et al.*, 2002]. Because the N_2 diffusion coefficient is lower than the O_2 and
262 Ar diffusion coefficients, the flux of N_2 from sea ice to the water is slower and, hence, the
263 incorporation rate of N_2 is larger than O_2 and Ar, leading to N_2 enrichment within sea ice.

264 Moreover, solubility of N_2 is only half the solubility of O_2 if nucleation process occurs at the ice-
265 water interface. This results in relatively more N_2 in the gas phase as compared with the other
266 gases. The growing ice will therefore be enriched in nitrogen bubbles that would otherwise have
267 diffused as a solute towards the water reservoir.

268

269 **5.2 Gas porosity, and bubble formation from brine supersaturation**

270 The estimated gas filled porosity (V_B) was 1 to 2.2% of the ice volume (Table A1). These
271 estimates are in the lower end of the estimates (1 to 5%) based on *Cox and Weeks* [1983], but are
272 close to the range (1.3 to 1.9%) reported by *Loose et al.* [2011]. Figure 4b shows that the total gas
273 content in sea ice is linearly related to bubble volume ($R^2=0.37$; $P\leq 0.01$, Figure 4b). We used this
274 relationship to infer that at $B=0$ (i.e. no bubbles are present), the total gas content (which must be
275 contained exclusively in the brines) would be approximately 5.6 ml kg^{-1} . This implies that gas

276 comes out of solution to form bubbles when the gas concentration in the brines exceeded this
277 value. The average air solubility of the brine medium was $2.06 \text{ ml kg}^{-1} \pm 0.91$ so nucleation within
278 the sea ice system appeared at saturation factor between 1.9 and 4.9. These results are
279 comparable to the findings of *Killawee et al.* [1998] in fresh water, who observed bubble
280 nucleation when saturation was between 2.2 and 2.5 times atmospheric saturation at the ice-water
281 interface. Note that the relatively low R^2 of the relationship between gas porosity and total gas
282 content (Figure 4b) is not surprising given the potential bias affecting both methods: First, total
283 gas content and C_B (which is used to reconstruct the gas filled porosity (V_B)) were measured on
284 two different cores; and secondly the C_B estimate is calculated from equation (1), in which
285 $C_{saturation}$ is derived from a brine volume fraction estimate that does not take into account the air
286 content (i.e. it is a simplification of the *Cox and Weeks* [1983] formulation).

287

288 **5.3 A first assessment of gas transport coefficients in sea ice at constant brine volume**

289 For each gas, we observed a decreasing peak with time at 27.5 cm below the ice surface (Figure
290 5). This gradual decrease of the gas concentration suggests that there was a gas movement within
291 the sea ice. The gases species displaced symmetrically from the highest concentration situated at
292 27.5 cm below the ice surface to lower concentration. Given the fact that the ice was not affected
293 by brine convection mechanisms (see section: 4.1 physical ice properties, Figure 3d.), the mode
294 of transportation was either through molecular diffusion in the brine (aqueous diffusion), or
295 bubble buoyancy. A distinguishing feature of diffusion is that it results in mixing or mass
296 transport, without requiring bulk motion. In the phenomenological approach, according to Fick's
297 laws, the diffusion flux is proportional to the negative gradient of concentrations. It goes from

298 regions of higher concentration to regions of lower concentration. The Fick's second law of
299 diffusion describes the change of concentration with time as:

300
$$\frac{\partial C_{bulk\ ice}}{\partial t} = D \left(\frac{\partial^2 C_{bulk\ ice}}{\partial z^2} + \frac{1}{A} \frac{\partial A}{\partial z} \frac{\partial C_{bulk\ ice}}{\partial z} \right) \quad (6)$$

301 Where $C_{bulk\ ice}$ is the bulk ice concentration in $\mu\text{mol L}^{-1}$ ($= \text{nmol cm}^{-3}$), t is the time in s, D is the
302 diffusion coefficient expressed in $\text{cm}^2 \text{s}^{-1}$, z is the length in cm, and A is the cross-sectional area
303 over which diffusion is occurring in cm^2 .

304
305 The diffusion of gas within sea ice is thought to occur through the network of brines. Assuming
306 the brine network can be described as a tube perpendicular to the ice cover (i.e z direction) of
307 section area, A ., the geometry of the problem is similar to decay of a pulse [Cussler, 2009, p34].
308 In the decay of pulse model the diffusion occurs away from a sharp pulse of solute (i.e the gas
309 peak at 27.5 cm below the ice surface). The initially steep concentration gradient weakens
310 gradually by diffusion in the z direction (i.e the brine channel perpendicular to the ice cover) into
311 the smooth curves.

312
313 For this first estimate of D -values, we assumed that diffusion occurs in a one-dimensional
314 medium of infinite length where the cross-sectional area is considered as constant. This cross
315 sectional area is the brine network and since the V_b only varied between 2 and 3% during the
316 sampling period we can assume, it was constant. Hence, the third term of the second Fick's law,

317 $\left(\frac{1}{A} \frac{\partial A}{\partial z} \frac{\partial C_{bulk\ ice}}{\partial z} \right)$ (equation 6)) is zero.

318
319 We approximated the vertical gas concentrations around the peak as a normal distribution (Figure
320 7) by applying a curve fit procedure that assumes that the concentrated solute was originally

321 located at $z = 0$ (i.e. 27.5 cm below the ice surface), and diffused as per the Gaussian profile
322 where the mathematical solution for the decay of pulse is given by:

$$323 \quad \bar{C} = \frac{M/A}{\sqrt{4\pi Dt}} e^{-z^2/4Dt} \quad (7)$$

324 where M is the total solute introduced in the system, A is the cross sectional area in cm, Z is the
325 length of the system over which the solute diffuses in cm, D is the diffusion coefficient expressed
326 in $\text{cm}^2 \text{s}^{-1}$ and t is the time expressed in s. The boundary conditions for this equation are as
327 follows: (1) far from the pulse, the solute concentration is zero: $t > 0$; $z = \infty$; $C = 0$; (2) because
328 diffusion occurs at the same speed in both directions (constant section), the pulse is symmetric;
329 (3) all of the solute is initially located at $z = 0$. At position $z=0$, the evolution of the peak
330 concentration over time is given by:

$$331 \quad C(0, t) = \frac{M}{\sqrt{4\pi Dt}} \times dz \quad (8)$$

332 Where dz is the length of the section on which the gas concentration is measured, 5 cm. $C(0,t)$ is
333 the gas concentration successively measured on March 13 and on March 15, 27.5 cm below the
334 ice surface ($Z=0$), (27.5, 13/03), $C(27.5, 15/03)$, respectively). M is the total quantity introduced
335 in the system, calculated from the maximum concentration observed on March 11, 27.5 cm below
336 the ice surface (Table A1)

337

338 From equation (8), we can then compute values of D for each gas species as:

$$339 \quad D = \frac{\left(\frac{M}{C(0,t)} \times dz\right)^2}{4\pi t} \quad (9)$$

340 In this first approach, computed D_{Ar} ranged from 1.54 to $1.76 \times 10^{-5} \text{ cm}^2 \text{ s}^{-1}$ ($\pm 17\%$), D_{O_2} from
341 1.54 to $1.77 \times 10^{-5} \text{ cm}^2 \text{ s}^{-1}$ ($\pm 11\%$), and D_{N_2} equal to $2.49 \times 10^{-5} \text{ cm}^2 \text{ s}^{-1}$ ($\pm 8\%$) (Table 3). We
342 computed D_{N_2} only for the first period because, the peak decreased faster and asymmetrically,
343 suggesting that other processes are involved.

344 **5.4 Gas diffusion pathways and bubble buoyancy**

345 As described above, there are two mechanisms for gas transport in sea ice in the absence of brine
346 convection: (1) the dissolved gas can diffuse in the brine solution following the concentration
347 gradient, or (2) the bubbles can move upward along the grain boundaries and in the brine network
348 under buoyancy [Loose *et al.*, 2011; Zhou *et al.*, 2013]. If bubbles are mobile, we expect (1) a
349 faster net gas transport (i.e. higher calculated diffusivities) and (2) a preferential apparent
350 diffusion in the positive (upward) direction. Our computed transport coefficients are of the same
351 magnitude as the aqueous molecular diffusion values (1 to $2 \times 10^{-5} \text{ cm}^2 \text{ s}^{-1}$) at similar
352 temperatures (Table 3). This suggests that the gas species primarily diffused through the brine
353 channels in the dissolved phase. However, according to equations (1) and (3) more than 70% of
354 the gas species were residing in bubbles (as a maximum estimate). The observed symmetrical
355 distribution of the gas around zone of the peak through time also suggests that the bubbles
356 remained immobile. An explanation for this observation is that the permeability of the bulk ice
357 was too low to allow for differential bubble movement under buoyancy. Zhou *et al.* [2013] have
358 recently demonstrated that brine volumes higher than 7% are necessary for bubble differential
359 movement in the brine network, as a result of tortuosity. Figure 3c shows that this condition was
360 not fulfilled above 50 cm depth (the area of interest), at least for the 11 and 13 March
361 measurements. The observed increase in brine volume fraction between 13 and 15 March is
362 consistent with higher calculated diffusivities (some bubbles might actually have escaped and
363 accumulated within the less permeable top 5 cm (Figures 3c and 5).

364
365 Overall, our estimates of the gas retained in bubbles as a proportion of bulk ice gas
366 concentrations, and the estimated gas filled porosities are probably overestimates. According to
367 Light *et al.* [2003], bubble nucleation is not only a function of the saturation level of the solution

368 but also of the size of the brine channel. Thus, a minimum brine channel size may be required to
369 form a stable bubble. Bubble nucleation should be successful for bubbles with radii sufficiently
370 large so that the surface tension is smaller than the internal tension of the brine [*Light et al.*,
371 2003]. On the other hand, the majority of bubbles observed by *Light et al.* [2003] were contained
372 within brine inclusions, and none were observed in the ice itself. Although the gases we
373 measured were primarily in the bubble phase, this does not exclude aqueous diffusion through the
374 brine medium. If the bubbles are contained within the brine inclusions, the gas-filled inclusions
375 are able to exchange gas with the brine and diffuse into the aqueous phase of the brine network.
376 A possible connection, and exchange, between gas-filled and liquid-filled porosities has also been
377 suggested by *Loose et al.* [2011].

378
379 The diffusivity of Ar and O₂ showed similar transport coefficients, and the same trend over time.
380 The values are also similar to those of *Wise & Houghton* [1966] in water at 10 °C (salinity not
381 specified), $1.7 \times 10^{-5} \text{ cm}^2 \text{ s}^{-1}$. However, the calculated D_{O_2} values are about 2 times lower than
382 those reported ($3.9 \times 10^{-5} \text{ cm}^2 \text{ s}^{-1} \pm 41\%$) by *Loose et al.* [2011] for sea ice with similar
383 porosities. Sea ice is a particularly heterogeneous environment, and the geometry and tortuosity
384 of the channels would be expected to have a substantial influence on gas migration, especially in
385 the form of bubble buoyancy. This is supported by the slight increase of D over time, which may
386 be related to the increasing brine volume allowing easier diffusion and/or easier bubbles
387 buoyancy. Therefore, it is not surprising that our values differ from those of *Loose et al.* [2011].
388 It also suggests that it may be desirable to establish a relationship between porosity and
389 molecular diffusion, but the available data do not cover a wide enough range of values to make
390 this feasible.

391

392 As mentioned previously, the calculated value of D_{N_2} was higher than D_{O_2} and D_{Ar} . However,
393 according to *Broecker & Peng* [1974] and *Stauffer et al.* [1985], D_{N_2} would be expected to be
394 lower than D_{O_2} . Moreover, the peak decreased less symmetrically. *Loose et al.* [2011], suggest a
395 multiphase-diffusion where transport of a part of the gas occur by liquid diffusion and another
396 part by gas diffusion, or by bubble buoyancy. This may accelerate the depletion of the gas
397 fraction because the bubble buoyancy is much faster than aqueous diffusion. Based on the
398 solubility coefficient (i.e. Bunsen, β), the gas species with the lowest solubility will be enriched
399 in the gas phase; which is referred to as “solubility partitioning”. O_2 is twice as soluble in water
400 compared with N_2 , and so the ability of N_2 to partition to the gas phase more readily would
401 provide it with a more rapid transport pathway and hence higher “apparent” diffusivities with an
402 assymmetric evolution of the gas peak. Note that this solubility partitioning could also be involved
403 in the chemical separation in the boundary layer during the ice growth. Thus, the supersaturation
404 level to initiate the nucleation process would be reached earlier for N_2 . The growing ice would be
405 enriched in nitrogen bubbles that would otherwise have diffused as a solute towards the water
406 reservoir. It is, however, not clear yet how such boundary layer processes are compatible with the
407 mushy layer approach for sea ice growth.

408 **6 Conclusion**

409 Our study investigated the transport of gas in natural sea ice in the absence of brine convection.
410 The low average bulk ice salinity (3.2) induced a stratified brine network, which prevented
411 convective exchanges through brines transport between the ice, water, and atmosphere. Hence, the
412 transport of gas species was mainly diffusive or buoyant. We used the temporal evolution of gas
413 distribution in sea ice to compute the bulk ice transport coefficients for Ar, N_2 and O_2 as
414 conservative dissolved gas tracers of mass transport.

415
416 Based on the total gas content (i.e included dissolved or gaseous gas species), the bulk ice
417 concentration of O₂, N₂, and Ar, and the gas filled porosity, we conclude that gas species are
418 preferentially located in bubbles. The gas incorporation at the ice-water interface occurred close
419 to the atmospheric solubility value, and the gas filled porosity was close to zero in the bottom of
420 the ice, hence, the nucleation process occurred mainly in the brines. Bubble nucleation requires
421 supersaturation of dissolved gas in the brines, and in this study the nucleation process was
422 observed once the concentration exceed 2.7 times the atmospheric saturation. This level of
423 supersaturation is in agreement with previous work on bubble nucleation in sea ice [e.g. *Killawee*
424 *et al.*, 1998].

425
426 The effective gas diffusion rates through sea ice observed in this study ranged from 1.54 to 1.76 ×
427 10⁻⁵ cm² s⁻¹ (±17%) for Ar, from 1.54 to 1.77 × 10⁻⁵ cm² s⁻¹ (±11%) for O₂, and was 2.49 × 10⁻⁵
428 cm² s⁻¹ (±8%) for N₂. We computed this transport rate over a narrow range of total porosity, 4 to
429 8%. It was therefore not possible to ascertain a relationship between porosity and the diffusion
430 coefficient, however, these experiments give some idea of the magnitude of *D* close the liquid
431 permeability threshold of 5%.

432
433 Although most gases were located in bubbles, the effective diffusivities for O₂, Ar and N₂ were
434 close to the aqueous diffusion rate (≈10⁻⁵ cm² s⁻¹). The preference for gases to exist in bubbles
435 does not exclude an aqueous diffusion through the brine medium. The majority of bubbles
436 observed by *Light et al.* [2003] were contained within brine inclusions; none were observed in the
437 ice itself. We hypothesize that the nucleation process occurs in the brine network and the gas-
438 filled inclusions are able to exchange with the brine and diffuse into the aqueous phase. This

439 work therefore extends to natural sea ice, the hypothesis that there is a connection and exchange
440 between gas-filled porosity and liquid-filled porosity, previously suggested by *Loose et al.*
441 [2011]. Finally, the preferential partitioning of N₂ into gas-filled pore spaces within the ice could
442 produce a greater apparent diffusion rate in comparison to O₂ and Ar, as well as a larger rate of
443 incorporation at the ice water interface during the initial freezing process.

444
445 **Acknowledgements.** We gratefully acknowledge the contributions of the Canada Excellence Research
446 Chair (CERC) and Canada Research Chair (CRC) programs. Support was also provided by the Natural
447 Sciences and Engineering Research (NSERC) Council, the Canada Foundation for Innovation and the
448 University of Manitoba. This work is a contribution to the ArcticNet Networks of Centres of Excellence
449 and the Arctic Science Partnership (ASP) *asp-net.org*. This work is also a contribution to the Belgian
450 FNRS-FRFC 2.4584.09 research contract. BD is a research associate of F.R.S.-FNRS. Participation by
451 DNT was made possible by The Royal Society, U.K. The authors would like to thank Saïda El Amri for
452 her efficient help in laboratory work.

453
454
455 **References:**

456
457 Broecker, W. S., and T. H. Peng (1974), Gas-exchange rates between air and sea, *Tellus*, 26(1-2),
458 21-35.

459
460 Carte, A. E. (1961), Air bubbles in ice, *Proceedings of the Physical Society*, 77(495), 757-768.

461 Cassar, N., B. A. Barnett, M. L. Bender, J. Kaiser, R. C. Hamme, and B. Tilbrook (2009),
462 Continuous High-Frequency Dissolved O₂/Ar Measurements by Equilibrator Inlet Mass
463 Spectrometry, *Anal. Chem.*, 81(5), 1855-1864.

464 Castro-Morales, K., N. Cassar, D. R. Shoosmith, and J. Kaiser (2013), Biological production in
465 the Bellingshausen Sea from oxygen-to-argon ratios and oxygen triple isotopes, *Biogeosciences*,
466 10(4), 2273-2291.

467
468 Cox, G. F. N., and W. F. Weeks (1983), Equations for determining the gas and brine volumes in
469 sea-ice samples, *Journal of Glaciology*, 29(102), 306 - 316.

470 Crabeck, O., Delille, B., Thomas, D. N., Geilfus, N. X., Rysgaard, S., and Tison, J. L.(2014),
471 CO₂ and CH₄ in sea ice from a subarctic fjord, *Biogeosciences Discuss.*, 11, 4047-4083,
472 doi:10.5194/bgd-11-4047-2014, 2014

473 Cussler. E.L (2009), Diffusion , Mass Transfert in fluid system, Cambridge University Press (3.
474 eds)

- 475 Eicken, H., M. A. Lange, and G. S. Dieckmann (1991), Spatial variability of sea ice properties in
476 the Northwestern Weddell Sea, *Journal of Geophysical Research-Oceans*, 96(C6), 10603-10615.
- 477 Else, B. G. T., T. N. Papakyriakou, R. J. Galley, W. M. Drennan, L. A. Miller, and H. Thomas
478 (2011), Wintertime CO₂ fluxes in an Arctic polynya using eddy covariance: Evidence for
479 enhanced air-sea gas transfer during ice formation, *J. Geophys. Res.*, 116, C00G03,
480 doi:10.1029/2010JC006760.
481
- 482 Garcia, H. E., and L. I. Gordon (1992), Oxygen solubility in seawater - better fitting equations,
483 *Limnology and Oceanography*, 37(6), 1307-1312.
- 484 Geilfus, N.-X., G. Carnat, T. Papakyriakou, J.-L. Tison, B. Else, H. Thomas, E. Shadwick, and B.
485 Delille (2012), Dynamics of pCO₂ and related air-ice CO₂ fluxes in the Arctic coastal zone
486 (Amundsen Gulf, Beaufort Sea), *J. Geophys. Res.*, 117, C00G10, doi:10.1029/2011JC007118.
487
- 488 Geilfus, N.-X., G. Carnat, G. S. Dieckmann, N. Halden, G. Nehrke, T. Papakyriakou, J.-L. Tison,
489 and B. Delille (2013), First estimates of the contribution of CaCO₃ precipitation to the release of
490 CO₂ to the atmosphere during young sea ice growth, *J. Geophys. Res. Oceans*, 118, 244-255,
491 doi:10.1029/2012JC007980.
492
- 493 Golden, K. M., S. F. Ackley, and V. I. Lytle (1998), The percolation phase transition in sea ice,
494 *Science*, 282(5397), 2238-2241.
- 495 Golden, K. M., H. Eicken, A. L. Heaton, J. Miner, D. J. Pringle, and J. Zhu (2007), Thermal
496 evolution of permeability and microstructure in sea ice, *Geophys. Res. Lett.*, 34, L16501,
497 doi:10.1029/2007GL030447.
498
- 499 Gosink, T. A., J. G. Pearson, and J. J. Kelly (1976), Gas movement through sea ice, *Nature*, 263,
500 41 - 42.
- 501 Hamme, R. C., and S. R. Emerson (2004), The solubility of neon, nitrogen and argon in distilled
502 water and seawater, *Deep-Sea Research Part I-Oceanographic Research Papers*, 51(11), 1517-
503 1528.
504
- 505 Heinesch, B., M. Yernaux, M. Aubinet, N. X. Geilfus, T. Papakyriakou, G. Carnat, H. Eicken, J.
506 L. Tison, and B. Delille (2009), Measuring air-ice CO₂ fluxes in the Arctic, *FluxLetter, The*
507 *Newsletter of FLUXNET*, 2(2), 9-10.
- 508 Kaartokallio, H., D. H. Sogaard, L. Norman, S. Rysgaard, J. L. Tison, B. Delille, and D. N.
509 Thomas (2013), Short-term variability in bacterial abundance, cell properties, and incorporation
510 of leucine and thymidine in subarctic sea ice, *Aquatic Microbial Ecology*, 71(1), 57-73.

- 511 Killawee, J. A., I. J. Fairchild, J. L. Tison, L. Janssens, and R. Lorrain (1998), Segregation of
512 solutes and gases in experimental freezing of dilute solutions: Implications for natural glacial
513 systems, *Geochimica Et Cosmochimica Acta*, 62(23-24), 3637-3655.
- 514 Langway, C. C. (1958), Ice fabrics and the universal stage Rep. 62, U.S. Snow, Ice and
515 Permafrost Research Establishment, Wilmette, Illinois.
- 516 Leppäranta, M., and T. Manninen (1988), The brine and gas content of sea ice with attention to
517 low salinities and high temperatures, *Rep.*, Helsinki.
- 518 Light, B., G. A. Maykut, and T. C. Grenfell (2003), Effects of temperature on the microstructure
519 of first-year Arctic sea ice, *J. Geophys. Res.*, 108, 3051, doi:[10.1029/2001JC000887](https://doi.org/10.1029/2001JC000887), C2.
520
- 521 Long, M. H., D. Koopmans, P. Berg, S. Rysgaard, R. N. Glud, and D. H. Sogaard (2012),
522 Oxygen exchange and ice melt measured at the ice-water interface by eddy correlation,
523 *Biogeosciences*, 9, 1-11.
- 524 Loose, B., W. R. McGillis, P. Schlosser, D. Perovich, and T. Takahashi (2009), Effects of
525 freezing, growth, and ice cover on gas transport processes in laboratory seawater experiments,
526 *Geophysical Research Letters*, 36(5), L05603.
- 527 Loose, B., P. Schlosser, D. Perovich, D. Ringelberg, D. T. Ho, T. Takahashi, J. Richter-Menge,
528 C. M. Reynolds, W. R. McGillis, and J. L. Tison (2011), Gas diffusion through columnar
529 laboratory sea ice: implications for mixed-layer ventilation of CO₂ in the seasonal ice zone,
530 *Tellus Series B-Chemical and Physical Meteorology*, 63(1), 23-39.
- 531 Lubetkin, S. D.(2003), Why is it much easier to nucleate gas bubbles than theory predicts?
532 *Langmuir*, 19, 2575– 258.
- 533 Matsuo, S., and Y. Miyake (1966), Gas composition in ice samples from Antarctica, *Journal of*
534 *Geophysical Research*, 71(22), 5235-5241.
- 535 Miller, L. A., T. N. Papakyriakou, R. E. Collins, J. W. Deming, J. K. Ehn, R. W. Macdonald, A.
536 Mucci, O. Owens, M. Raudsepp, and N. Sutherland (2011), Carbon dynamics in sea ice: A winter
537 flux time series, *J. Geophys. Res.*, 116, C02028, doi:[10.1029/2009JC006058](https://doi.org/10.1029/2009JC006058).
538
- 539 Millero F.J ,(1978) ; Freezing point of seawater 8th Report of JPOTS, Unesco technical papers in
540 marine science, 28, UNESCO.
- 541
- 542 Mock, T., G. S. Dieckmann, C. Haas, A. Krell, J. L. Tison, A. L. Belem, S. Papadimitriou, and D.
543 N. Thomas (2002), Micro-optodes in sea ice: a new approach to investigate oxygen dynamics
544 during sea ice formation, *Aquatic Microbial Ecology*, 29(3), 297-306.

545 Mortensen, J., K. Lennert, J. Bendtsen, and S. Rysgaard (2011), Heat sources for glacial melt in a
546 sub-Arctic fjord (Godthåbsfjord) in contact with the Greenland Ice Sheet, *J. Geophys. Res.*, 116,
547 C01013, doi:[10.1029/2010JC006528](https://doi.org/10.1029/2010JC006528).

548 Nomura, D., H. Yoshikawa-Inoue, and T. Toyota (2006), The effect of sea-ice growth on air-sea
549 CO₂ flux in a tank experiment, *Tellus Series B-Chemical and Physical Meteorology*, 58(5), 418-
550 426.
551

552 Nomura, D., H. Yoshikawa-Inoue, T. Toyota, and K. Shirasawa (2010), Effects of snow, snow-
553 melting and re-freezing processes on air-sea ice CO₂ flux, *Journal of Glaciology*, 56(196), 262-
554 270.
555

556 Notz, D., and M. G. Worster (2008), In situ measurements of the evolution of young sea ice, *J.*
557 *Geophys. Res.*, 113, C03001, doi:[10.1029/2007JC004333](https://doi.org/10.1029/2007JC004333).
558

559 Papadimitriou, S., H. Kennedy, L. Norman, D. P. Kennedy, G. S. Dieckmann, and D. N. Thomas
560 (2012), The effect of biological activity, CaCO₃ mineral dynamics, and CO₂ degassing in the
561 inorganic carbon cycle in sea ice in late winter-early spring in the Weddell Sea, Antarctica, *J.*
562 *Geophys. Res.*, 117, C08011, doi:[10.1029/2012JC008058](https://doi.org/10.1029/2012JC008058).
563

564 Papakyriakou, T., and L. Miller (2011), Springtime CO₂ exchange over seasonal sea ice in the
565 Canadian Arctic Archipelago, *Annals of Glaciology*, 52(57), 215-224.

566 Raynaud, D., R. Delmas, M. Ascencio, and M. Legrand (1982), Gas extraction from polar ice
567 cores: a critical issue for studying the evolution of atmospheric CO₂ and ice-sheet surface
568 elevation, *Annals of Glaciology*, 3, 265-268.

569 Rysgaard, S., and R. N. Glud (2004), Anaerobic N₂ production in Arctic sea ice, *Limnology and*
570 *Oceanography*, 49(1), 86-94.

571 Rysgaard, S., R. N. Glud, M. K. Sejr, J. Bendtsen, and P. B. Christensen (2007), Inorganic carbon
572 transport during sea ice growth and decay: A carbon pump in polar seas, *J. Geophys. Res.*, 112,
573 C03016, doi:[10.1029/2006JC003572](https://doi.org/10.1029/2006JC003572).
574

575 Rysgaard, S., R. N. Glud, M. K. Sejr, M. E. Blicher, and H. J. Stahl (2008), Denitrification
576 activity and oxygen dynamics in Arctic sea ice, *Polar Biol.*, 31, 527-537.

577 Shaw, M. D., L. J. Carpenter, M. T. Baeza-Romero, and A. V. Jackson (2011), Thermal evolution
578 of diffusive transport of atmospheric halocarbons through artificial sea-ice, *Atmos. Environ.*,
579 45(35), 6393-6402.

580 Skoog, D. A., D. M. West, and F. J. Holler (1997), *Chimie Analytique*, De Boeck Universit_e,
581 Paris, Bruxelles.
582

583 Sogaard, D. H., D. N. Thomas, S. Rysgaard, R. N. Glud, L. Norman, H. Kaartokallio, T. Juul-
584 Pedersen, and N. X. Geilfus (2013), The relative contributions of biological and abiotic processes
585 to carbon dynamics in subarctic sea ice, *Polar Biol.*, 36(12), 1761-1777.
586

587 Sørensen, B. L. L., Jensen, R. N. Glud, D. F. McGinnis, M. K. Sejr J. Sievers, D. H. Sogaard, J.-
588 L. Tison, and S. Rysgaard, (2013) : Parameterization of atmosphere–surface exchange of CO₂
589 over sea ice, *The Cryosphere Discuss.*, 7, 3899–3929, doi:10.5194/tcd-7-3899-2013
590

591 Stauffer, B., A. Neftel, H. Oeschger, and J. Schwander (Eds.) (1985), *CO₂ concentration in air*
592 *extracted from Greenland ice samples*, 85-89 pp., Geophysical Monograph Washington DC.

593 Stefels, J., G. Carnat, J. W. H. Dacey, T. Goossens, J. T. M. Elzenga, and J.L. Tison (2012), The
594 analysis of dimethylsulfide and dimethylsulfoniopropionate in sea ice: Dry-crushing and melting
595 using stable isotope additions, *Mar. Chem.*, 128–129, 34–43.

596 Tison, J. L., C. Haas, M. M. Gowing, S. Sleewaegen, and A. Bernard (2002), Tank study of
597 physico-chemical controls on gas content and composition during growth of young sea ice,
598 *Journal of Glaciology*, 48(161), 177-191.

599 Tison, J. L., A. Worby, B. Delille, F. Brabant, S. Papadimitriou, D. Thomas, J. de Jong, D.
600 Lannuzel, and C. Haas (2008), Temporal evolution of decaying summer first-year sea ice in the
601 Western Weddell Sea, Antarctica, *Deep-Sea Research Part II-Topical Studies in Oceanography*,
602 55(8-9), 975-987.

603 Tsurikov, V. L. (1979), The formation and composition of the gas content of sea ice, *Journal of*
604 *Glaciology*, 22(86), 67 - 81.

605 UNESCO (1978), Eight report of the joint panel on oceanographic tables and standards,
606 *Technical papers in Marine Science*, 28.

607 Vancoppenolle, M., H. Goosse, A. de Montety, T. Fichefet, B. Tremblay, and J. L. Tison (2010),
608 Modeling brine and nutrient dynamics in Antarctic sea ice: The case of dissolved silica, *J.*
609 *Geophys. Res.*, 115, C02005, doi:10.1029/2009JC005369.
610

611 Wise, D. L., and G. Houghton (1966), Diffusion coefficients of 10 slightly soluble gases in water
612 at 10-60 degrees c, *Chemical Engineering Science*, 21(11), 999-&.

613 Zemelink, H. J., B. Delille, J. L. Tison, E. J. Hints, L. Houghton, and J. W. H. Dacey (2006),
614 CO₂ deposition over the multi-year ice of the western Weddell Sea, *Geophys. Res. Lett.*, 33,
615 L13606, doi:10.1029/2006GL026320.
616

617 Zhou, J. Y., B. Delille, H. Eicken, M. Vancoppenolle, F. Brabant, G. Carnat, N. X. Geilfus, T.
618 Papakyriakou, B. Heinesch, and J. L. Tison (2013), Physical and biogeochemical properties in

619 landfast sea ice (Barrow, Alaska): Insights on brine and gas dynamics across seasons, *Journal of*
620 *Geophysical Research-Oceans*, 118(6), 3172-3189.

621

622 **List of tables:**

623

624 **Table 1:** Relative proportion of O₂, Ar and N₂ in landfast sea ice at Kapisillit

625

626 **Table 2:** Saturation factor, (Sat_f), computed following the equation 2

627 **Table 3:** Diffusivity coefficients deduced from equations (8) and (9). and comparison reference

628 values in the literature.

629

630 **List of Figures**

631 **Figure 1.** Schematic view of gas entrapment and evolution in sea ice. During the freezing process
632 the expelled dissolved gases are trapped in the brine solution, or in bubbles that are released at
633 the ice-water interface. Increased concentration of the brines by freezing results in further
634 formation of gas bubbles by nucleation processes. The main transport processes of gas within the
635 sea ice depend on the permeability and convection threshold given by the brine volume and the
636 Rayleigh number. If V_b is under 5%, no convection occurs in sea ice and gas transport is
637 controlled by diffusion process. During diffusion, the gas can be released both into the underlying
638 water and to the atmosphere as a function of the gradient concentration. While V_b is above 5%
639 and $Ra > 5$ or 10, brine convection occur and brine can exchange with the seawater underneath. If
640 the V_b exceeds 7.5%, bubbles are able migrate upward and gas maybe released to the atmosphere.

641 **Figure 2.** Study site –Landfast sea ice in Godthåbsfjord, SW Greenland. Circle includes the Bay
642 with the study site and the settlement Kapisillit.

643

644 **Figure 3. (a)** Bulk ice salinity, S_i **(b)** Temperature, **(c)** Brine volume fraction or liquid filled
645 porosity, V_b . The vertical dashed line is a reference value for the permeability threshold
646 according to Golden et al. 1998, 2007, **(d)** Rayleigh number, Ra , the dotted lines are a reference
647 value for the convection threshold according to Notz and Worster (2008) and Vancopenolle et al.
648 (2010) respectively.

649
 650 **Figure 4. (a)** Evolution of the total gas content in bulk sea ice as compared to solubility in brine
 651 at atmospheric saturation (white circle; air solubility). **(b)** Relationship between the total gas
 652 content measured with the toepler pump and the computed gas filled porosity (V_B). A regression
 653 line is shown ($r^2=0,37$, $P<0,001$) and its intersection with the y axis represent the maximum
 654 volume of dissolved gas in the brines.

655
 656 **Figure 5.** Evolution of Ar, O₂ and N₂ concentrations in bulk sea ice as compared to the
 657 concentration at atmospheric saturation (white triangle).

658
 659 **Figure 6.** Relationship between N₂, O₂ and Ar in the sea ice samples. The solid line is the
 660 regression line. The solid line represents the sea water ratios (N₂:Ar, O₂:Ar, N₂: O₂) while the
 661 dashed line represents the atmospheric ratios (N₂:Ar, O₂:Ar, N₂: O₂).

662
 663 **Figure 7.** Best-fit curves of the gas peak situated at 27.5 cm below the ice surface. For each
 664 species the concentration distribution are approximated by a Gaussian curve fit with 3
 665 parameters.

666

667 **List of Tables :**

668 **Table 1:** Relative proportion of O₂, Ar and N₂ in landfast sea ice at Kapisilit

Gas composition (%)	O ₂		Ar		N ₂	
	Min	Max	Min	Max	Min	Max
11 March	22.7	32.7	0.94	1.28	68.2	76.3
13 March	23.9	31.4	0.970	1.25	67.2	75.1
15 March	24.1	30.5	0.973	1.29	68.2	74.9
Sea ice <i>Tsurikov</i> [1979]	20.6	29.0	0.9	1.1	54.2	76.8
Sea ice <i>Tison et al.</i> [2002]	24.36	30.46	nd	nd	69.54	78.08
Sea water (t= 0 °C, S=33)	34.84		1.69		61.14	
Atmospheric composition	20.95		0.93		78.08	

669 **Table 2:** Saturation factor, (Sat_f), computed following the equation 2

Gas species	Saturation factor ($C_{bulk\ ice}/C_{saturation}$)	
	MIN	Max
O ₂	0.64	20.2
Ar	0.52	18.5
N ₂	0.82	39

670
671 **Table 3:** Diffusivity coefficients deduced from equations (8) and (9). and comparison reference values in the litterature.

Data			
Gas peak 27.5 (cm) Z=0	11 March M	13 March C (0, 13/03)	15 March C (0,15/03)
[Ar] $\mu\text{mol L}^{-1}$ ice	11.66	10.7	8.13
[O ₂] $\mu\text{mol L}^{-1}$ ice	275.3	236.9	192.5
[N ₂] $\mu\text{mol L}^{-1}$ ice	750.1	509.6	429.8
Results			
Diffusion in sea ice	D _{Ar} 10 ⁻⁵ cm ² s ⁻¹	D _{O₂} 10 ⁻⁵ cm ² s ⁻¹	D _{N₂} 10 ⁻⁵ cm ² s ⁻¹
Kapisilit (-2 <T (°C)< -5,4%<V _b <8.05%)	1.54-1,76 (± 17%)	1.55-1.74 (± 9%)	2.49 (± 11%)
References			
Diffusion in water	D _{Ar} 10 ⁻⁵ cm ² s ⁻¹	D _{O₂} 10 ⁻⁵ cm ² s ⁻¹	D _{N₂} 10 ⁻⁵ cm ² s ⁻¹
Broecker & Peng [1974] (T=0 °C)	0.88	1.17	0.95
Stauffer et al. [1985] (T=0 °C)	Na	2.08	1.61
Wise & Houghton [1966] (T=10 °C)	1.7	1.7	1.8
Diffusion in sea ice	D _{SF₆} 10 ⁻⁵ cm ² s ⁻¹	D _{O₂} 10 ⁻⁵ cm ² s ⁻¹	D _{CO₂} 10 ⁻⁵ cm ² s ⁻¹
Gosink et al. [1976] (-15>T (°C)< -7)	0.9	Na	40
Loose et al. [2011] (-4 <T (°C)< -12, 6%<V _b <8%)	13 (±40%)	3.9 (±41%)	na
Diffusion in gas phase (Cusller, 3 ed , 2009)	10 ⁻¹ cm ² s ⁻¹		

673
674 **Appendix**
675 **Table 1:** Temporal evolution of sea ice properties at the gas maximum. The reported values are sea ice temperature (T),
676 relative brine volume (V_b), bulk ice gas concentration ($C_{bulk\ ice}$), saturation concentration in brine ($C_{saturation}$), gas

677 concentration in bubbles (C_B), the fraction of gas content in bubble (f_B), the bubble volume (B), and relative bubble volume
 678 or gas filled porosity (V_B).

	Mean depth (cm)		
	22.5	27.5	32.5
a. 11 March			
T(°C)	-2.59	-2.54	-2.54
Bulk Salinity	2.25	3.12	3.37
V_b (%)	4.2	5.97	6.45
$C_{bulk\ ice}, O_2$ ($\mu\text{mol L}^{-1}$ ice)	185.34	275.30	138.46
$C_{bulk\ ice}, N_2$ ($\mu\text{mol L}^{-1}$ ice)	556.15	750.16	356.72
$C_{bulk\ ice}, Ar$ ($\mu\text{mol L}^{-1}$ ice)	8.06	11.66	6.10
$C_{saturation}, O_2$ ($\mu\text{mol L}^{-1}$ ice)	13.29	18.97	20.50
$C_{saturation}, N_2$ ($\mu\text{mol L}^{-1}$ ice)	23.43	33.48	36.18
$C_{saturation}, Ar$ ($\mu\text{mol L}^{-1}$ ice)	0.65	0.92	1.00
C_B, O_2 ($\mu\text{mol L}^{-1}$ ice)	172.05	256.32	117.96
C_B, N_2 ($\mu\text{mol L}^{-1}$ ice)	532.72	716.68	320.54
C_B, Ar ($\mu\text{mol L}^{-1}$ ice)	7.42	10.74	5.10
f_B, O_2 (%)	92.83	93.11	85.19
f_B, N_2 (%)	95.79	95.54	89.86
f_B, Ar (%)	91.97	92.07	83.61
B, O_2 (L gas L ⁻¹ ice)	0.0038	0.0057	0.0026
B, N_2 (L gas L ⁻¹ ice)	0.0118	0.0159	0.0071
B, Ar (L gas L ⁻¹ ice)	0.0002	0.0002	0.0001
V_B (%)	1.6	2.22	0.98
Total Porosity (air+brine) (%)	5.78	8.15	7.43

679
680

	Mean depth gas (cm)		
	22.5	27.5	32.5
b. 13 March			
T(°C)	-3.26	-2.92	-2.61
Bulk Salinity	2.74	2.67	3.96
V_b (%)	4.00	4.48	7.36
$C_{bulk\ ice}, O_2$ ($\mu\text{mol L}^{-1}$ ice)	156.98	236.99	104.47
$C_{bulk\ ice}, N_2$ ($\mu\text{mol L}^{-1}$ ice)	502.57	509.60	238.42
$C_{bulk\ ice}, Ar$ ($\mu\text{mol L}^{-1}$ ice)	6.461	10.07	3.95
$C_{saturation}, O_2$ ($\mu\text{mol L}^{-1}$ ice)	11.94	13.66	23.21
$C_{saturation}, N_2$ ($\mu\text{mol L}^{-1}$ ice)	20.89	24.00	40.92
$C_{saturation}, Ar$ ($\mu\text{mol L}^{-1}$ ice)	0.58	0.66	1.13
C_B, O_2 ($\mu\text{mol L}^{-1}$ ice)	145.04	223.26	81.27
C_B, N_2 ($\mu\text{mol L}^{-1}$ ice)	481.69	485.60	197.51
C_B, Ar ($\mu\text{mol L}^{-1}$ ice)	5.88	9.40	2.82

f_B, O_2 (%)	92.39	94.23	77.78
f_B, N_2 (%)	95.84	95.28	82.83
f_B, Ar (%)	90.99	93.38	71.33
B, O_2 (L gas L ⁻¹ ice)	0.0032	0.0049	0.0018
B, N_2 (L gas L ⁻¹ ice)	0.0107	0.0108	0.0044
B, Ar (L gas L ⁻¹ ice)	0.0001	0.0002	0.0001
V_B (%)	1.40	1.59	0.62
Total Porosity (air+brine) (%)	5.45	6.07	7.98

681

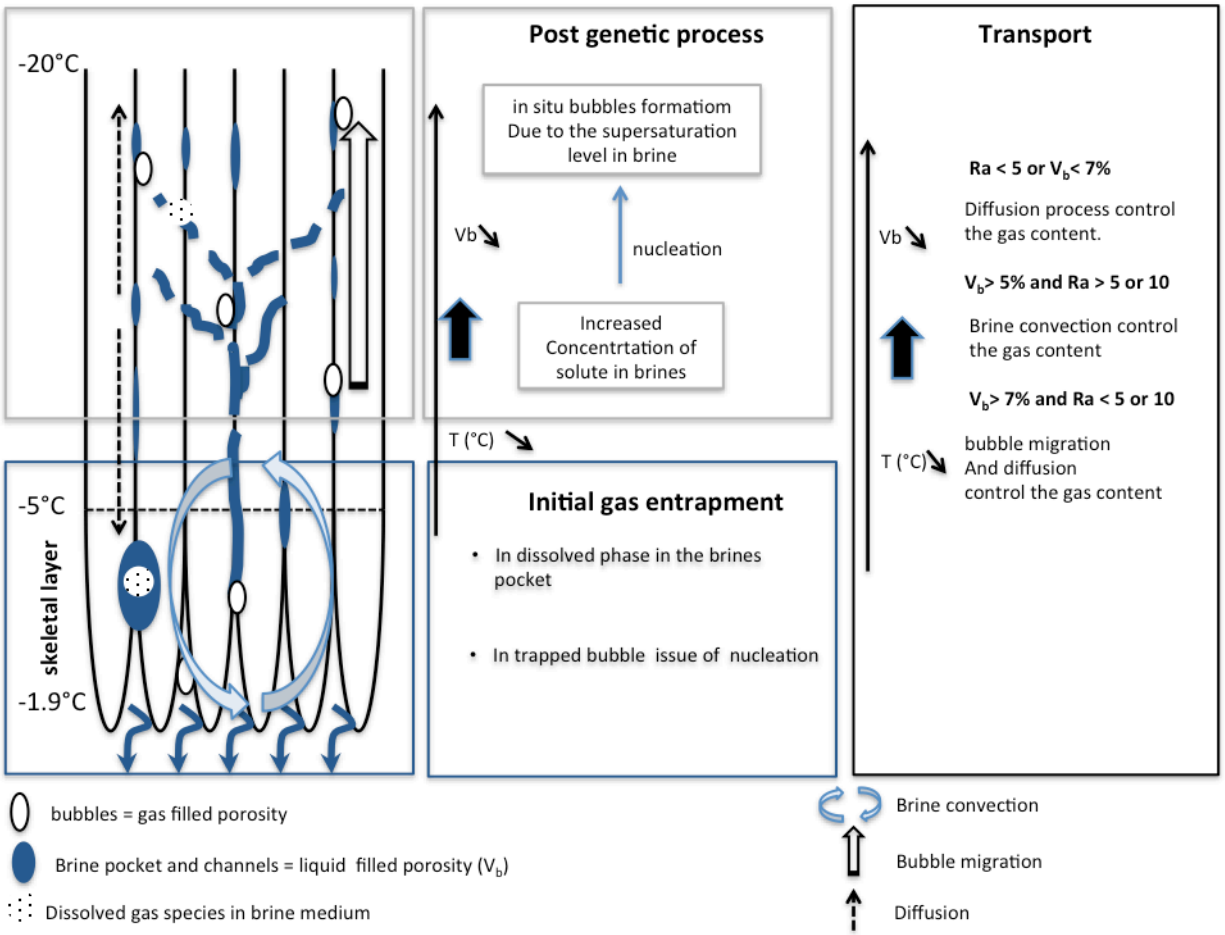
c. 15 March	Mean depth gas (cm)		
	22.5	27.5	32.5
T(°C)	-2.24	-2.46	-2.34
Bulk Salinity	2.72	3.42	3.95
V_b (%)	5.93	6.75	8.05
$C_{bulk\ ice}, O_2$ (μmol L ⁻¹ ice)	157.39	192.53	175.34
$C_{bulk\ ice}, N_2$ (μmol L ⁻¹ ice)	402.63	429.87	463.61
$C_{bulk\ ice}, Ar$ (μmol L ⁻¹ ice)	6.16	8.14	7.16
$C_{saturation}, O_2$ (μmol L ⁻¹ ice)	19.45	21.64	26.13
$C_{saturation}, N_2$ (μmol L ⁻¹ ice)	34.44	38.21	46.22
$C_{saturation}, Ar$ (μmol L ⁻¹ ice)	0.95	1.05	1.27
C_B, O_2 (μmol L ⁻¹ ice)	137.95	170.89	149.21
C_B, N_2 (μmol L ⁻¹ ice)	368.19	391.66	417.39
C_B, Ar (μmol L ⁻¹ ice)	5.22	7.08	5.88
f_B, O_2 (%)	87.64	88.76	85.10
f_B, N_2 (%)	91.45	91.11	90.03
f_B, Ar (%)	84.61	87.04	82.20
B, O_2 (L gas L ⁻¹ ice)	0.0031	0.0038	0.0033
B, N_2 (L gas L ⁻¹ ice)	0.0082	0.0087	0.0092
B, Ar (L gas L ⁻¹ ice)	0.0001	0.0002	0.0001
V_B (%)	1.13	1.26	1.27
Total Porosity (air+brine) (%)	7.06	8.01	9.32

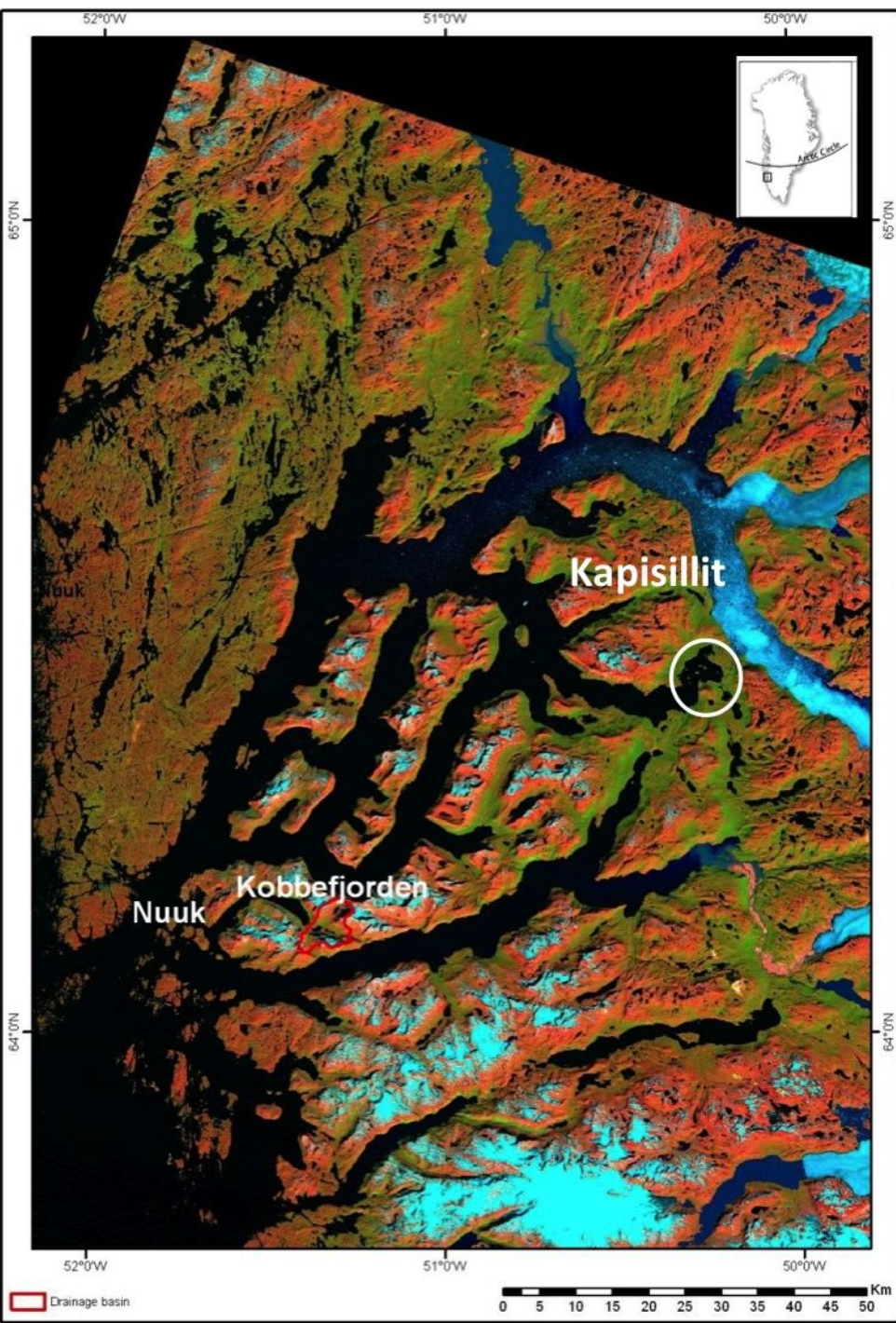
682

683

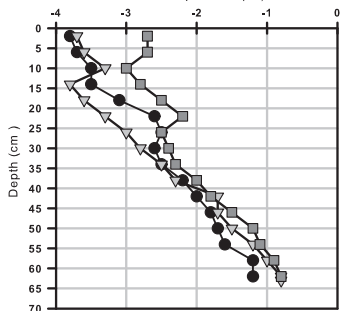
684

685

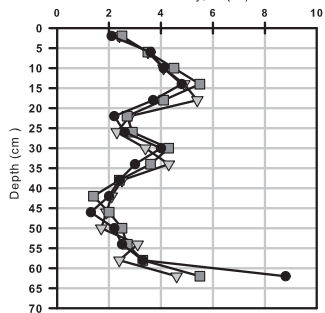
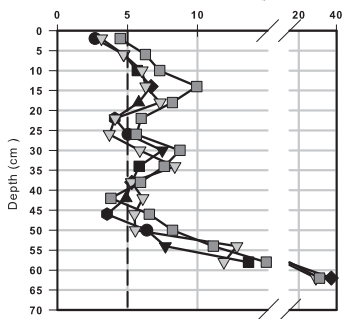




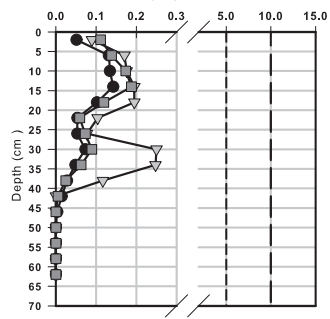
a. Temperature (C°)



b. Bulk ice salinity, Si (‰)

c. Brine Volume fraction V_b (%)

d. Rayleigh Number, Ra



- 11 March
- △ 13 March
- 15 March
- - - Permeability threshold (Golden et al., 1998)
- Ra threshold (Notz & Worster, 2008)
- - - Ra threshold (Vancoppenolle et al., 2010)

